Bioelectrochemistry 156 (2024) 108595

Contents lists available at ScienceDirect

Bioelectrochemistry

journal homepage: www.journals.elsevier.com/bioelectrochemistry

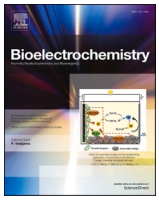

Polyethylene glycol hydrogel coatings for protection of electroactive bacteria against chemical shocks

Niloufar Fattahi [a], Jeffrey Reed [a], Evan Heronemus [b], Priyasha Fernando [b], Ryan Hansen [a,*], Prathap Parameswaran [b,*]

[a] Tim Taylor Department of Chemical Engineering, Kansas State University, Manhattan, KS 66506, USA
[b] Department of Civil Engineering, Kansas State University, Manhattan, KS 66506, USA

ARTICLE INFO

Keywords:
Hydrogels
Polyethylene glycol
Bioelectrochemical systems
Microbial electrolysis cells
Cell encapsulation

ABSTRACT

Loss of bioelectrochemical activity in low resource environments or from chemical toxin exposure is a significant limitation in microbial electrochemical cells (MxCs), necessitating the development of materials that can stabilize and protect electroactive biofilms. Here, polyethylene glycol (PEG) hydrogels were designed as protective coatings over anodic biofilms, and the effect of the hydrogel coatings on biofilm viability under oligotrophic conditions and ammonia-N (NH_4^+-N) shocks was investigated. Hydrogel deposition occurred through polymerization of PEG divinyl sulfone and PEG tetrathiol precursor molecules, generating crosslinked PEG coatings with long-term hydrolytic stability between pH values of 3 and 10. Simultaneous monitoring of coated and uncoated electrodes co-located within the same MxC anode chamber confirmed that the hydrogel did not compromise biofilm viability, while the coated anode sustained nearly a 4 × higher current density (0.44 A/m^2) compared to the uncoated anode (0.12 A/m^2) under oligotrophic conditions. Chemical interactions between NH_4^+-N and PEG hydrogels revealed that the hydrogels provided a diffusive barrier to NH_4^+-N transport. This enabled PEG-coated biofilms to generate higher current densities during NH_4^+-N shocks and faster recovery afterwards. These results indicate that PEG-based coatings can expand the non-ideal chemical environments that electroactive biofilms can reliably operate in.

1. Introduction

Microbial electrochemical cells (MxCs) are an emerging, sustainable environmental biotechnology platform that could produce renewable energy, recover carbon and nutrients as valorized products, and synthesize chemicals for societal use [1–3]. Other relevant applications of MxCs include biosensing, capacitors for remote sensing, and sub-surface remediation of contaminants. Anode-respiring bacteria (ARB) are microorganisms that form the anodic biofilm and are capable of transferring electrons from an electrode by consuming simple organic substrates, such as acetate, to produce electric current [4]. ARB are essential for MxC application, however long-term sustenance of ARB in the biofilm anode is dependent on ecological interactions with other anaerobic microbes and their ability to resist enviromental perturbations in pH, temperature, dissolved oxygen, and toxins such as heavy metals, bleach, ammonia-N, and oxidants such as hydrogen peroxide.

Resistance to toxic constituents in organic waste streams is of particular significance if MxCs are to serve in any of the aforementioned applications. For example, animal waste streams are a significant fraction of biomass waste resources in the United States [5]. These streams are characterized by high total ammonia nitrogen (TAN) concentrations, the total sum of NH_3 and ammonium-N (NH_4^+-N) ion in the aqueous phase. These waste streams, along with side stream municipal wastewater sources, are viable niches for the application of MxCs for waste valorization. TAN levels in these streams can range between 2000 and 8000 mg N/L [6], which severely hampers the methanogenesis phase of anaerobic digestion [7], and the sustained performance of MxC anodes for energy recovery or other long-term applications. Prior research has shown that ARB metabolic activity is severely impacted when exposed to NH_4^+-N concentrations above 3 g/L [8]. Hence, there is a need to either acclimatize the anode biofilms to the high concentrations of NH_4^+-N or develop anodic materials that provide ARB protection against NH_4^+-N exposure.

Recently, interfacing anode-bound ARB biofilms with hydrogel

* Corresponding authors.
E-mail addresses: rrhansen@ksu.edu (R. Hansen), prathapp@ksu.edu (P. Parameswaran).

https://doi.org/10.1016/j.bioelechem.2023.108595
Received 18 July 2023; Received in revised form 25 October 2023; Accepted 30 October 2023
Available online 8 November 2023

materials has been demonstrated to improve various aspects of MxC performance. Due to their porous structure, high water content, and biocompatibility, hydrogels can be designed to control mass transport, enhance cell colonization, cell metabolic activity, and electron transfer in the anode environment. Most efforts in this area have focused on developing conductive hydrogels to enhance extracellular electron transport from individual cells or biofilms to the electrode, addressing the limited power generation traditionally associated with MxCs [9,10]. Hydrogels containing conductive polypyrroles [11], ferrocene [12], TiO_2 [13], graphene oxide [14], carbon nanotubes [15], and gold nanoparticles [16] have been reported to improve current density and power output. Fewer reports demonstrate the use of hydrogels to protect ARB against environmental stressors. Du *et al.* encapsulated ARB with polydopamine for protection against extreme acid shock [17], while Luo *et al.* used agarose hydrogels to prevent exogenous bacteria from disrupting the function of ARB biofilms on the anode [18], and Li *et al.* used poly(vinyl alcohol) coatings to create anaerobic conditions at the biofilm-electrode interface during operation in an aerobic environment [19]. These studies provide impetus for further exploration of hydrogel materials as protective coatings for improved MxC performance.

Polyethylene glycol (PEG) based hydrogels are well-developed biomaterials used in a multitude of applications in drug delivery [20], mammalian cell culture [21], and biosensing [22]. PEG based hydrogels have also been developed as interfaces for microbial systems, most notably as antifouling surfaces [23,24] and recently as materials that can encapsulate and isolate bacteria with rare or unique function [25–30]. However, their use as an ARB interface material has not been well-explored. PEG is potentially advantageous in this application, as it is chemically inert, biocompatible, and because a wide variety of PEG precursors with different molecular weights and end group chemistries are commercially available. Precursor solutions that react together in the presence of cells through highly specific "click" chemistries can therefore be used to design and fabricate hydrogels with well-controlled mesh sizes for control of mass transfer [31–34]. Chemical or biological functionality can be added to PEG hydrogels by co-polymerizing or encapsulating reactive components into the hydrogel matrix or by targeting reactive end-groups after hydrogel formation [30]. With these advantages, PEG-based hydrogels were investigated here as protective coatings for ARB biofilms. Coatings were designed to remain physically stable on anode surfaces, chemically stable across a range of pH values, and to provide sufficient transport of nutrients to the biofilm interface to maintain ARB viability. Side-by-side comparison of coated and uncoated anode biofilm performance in an MxC were performed under two unique non-ideal environments: low substrate (oligotrophic) concentrations, as well as during and after NH_4^+-N shocks, as occurs in animal wastewaters. The findings from these experiments indicate that the hydrogel coatings can enable more robust operation of MxCs in non-ideal chemical environments, particularly environments where oligotrophic conditions or repeated exposure to high concentrations of chemical toxins can occur.

2. Materials and methods

2.1. Materials

Pentaerythritol tetra (mercaptoethyl) polyoxyethylene (PEG-tetrathiol or PEGTT, MW 10,000 Da) was purchased from NOF America Corporation (White Plains, NY). PEG-divinyl sulfone (PEGVS, MW 3400 Da) was purchased from Creative PEGWorks (Chapel Hill, NC). (3-Mercaptopropyl) trimethoxysilane, sodium phosphate monobasic dihydrate ($NaH_2PO_4{\cdot}2H_2O$), sodium hydroxide (NaOH), alconox detergent, toluene anhydrous, sodium hydrogen phosphate (Na_2HPO_4), potassium phosphate monobasic (KH_2PO_4), ammonium chloride (NH_4Cl), ethylene diamine tetraacetic acid (EDTA), cobalt chloride hexahydrate ($CoCl_2{\cdot}6H_2O$), calcium chloride dihydrate ($CaCl_2{\cdot}2H_2O$), boric acid (H_3BO_3), sodium molybdate dihydrate ($Na_2MoO_4{\cdot}2H_2O$), sodium selenite (Na_2SeO_3), sodium tungstate dihydrate ($Na_2WO_4{\cdot}2H_2O$), nickel chloride hexahydrate ($NiCl_2{\cdot}6H_2O$), magnesium chloride ($MgCl_2$), manganese chloride tetrahydrate ($MnCl_2{\cdot}4H_2O$), zinc chloride ($ZnCl_2$), copper sulfate pentahydrate ($CuSO_4{\cdot}5H_2O$) and aluminum potassium sulfate ($AlK(SO_4)_2$), ferrous chloride ($Fe(II)Cl_2$), sodium sulfide nonahydrate ($Na_2S{\cdot}9H_2O$), and sodium hydroxide (NaOH) were purchased from Sigma-Aldrich (St. Louis, MO). Rectangular graphite electrodes were ordered from GraphiteStore (Northbrook, IL). Ag/AgCl reference electrodes were purchased from BASi (West Lafayette, IN).

2.2. Hydrogel crosslinking chemistry and hydrogel hydrolytic stability experiments

The long-term hydrolytic stability of PEG hydrogels formed with thiol-vinyl sulfone click chemistry using PEGVS and PEGTT precursors was first investigated at pH values of 3, 7, and 10 using gravimetric analysis as described by Paez *et al.* [35]. For comparison, PEG hydrogels formed using PEGTT and PEG diacrylate (PEGDA) precursors were compared, as these hydrogels are susceptible to hydrolysis due to the presence of ester moieties in acrylates groups [36]. All hydrogels were prepared by pipetting 95 μL of hydrogel precursor solution which contained thiol groups and VS or acrylate groups at 22 mM. After mixing, precursor solutions were placed on a flat parafilm surface for 25 min (min) to allow for gelation. Hydrogels were then immersed in Milli-Q water at room temperature for 48 hours (h) to allow for swelling and to reach equilibrium, the initial mass of swollen hydrogels was then measured. Hydrogels were then incubated in citric buffer (pH 3), phosphate buffer (pH 7), and carbonate buffer (pH 10) for 72 days at room temperature. The mass of the swollen hydrogels was measured at varied time points, and the normalized mass of swollen hydrogels at individual time points was calculated as the hydrogel mass at each time ($m_{h,t}$) divided by the initial hydrogel mass ($m_{h,o}$). Increases in N_m from 1.0 indicate swelling in the hydrogel due to degradation of covalent crosslinks [35]. Hydrogel degradation was measured in triplicate for each condition.

2.3. Diffusion coefficient (D) and partition coefficient (K_D) measurements

To assess mass transport throughout the PEG hydrogels, experimental measurement of diffusion coefficients of the carbon source (acetate) through the PEG hydrogels ($\boldsymbol{D_{A,PEG}}$) and of ammonium (NH_4-N) through the PEG hydrogels ($\boldsymbol{D_{N,PEG}}$) was required. To quantify diffusivities, a cylindrical hydrogel was loaded with an analyte and placed in a glass cylinder to create perfect sink conditions and axial diffusion only, as release from the edges or bottom of the cylindrical hydrogel cannot occur (**Fig. S1**). The analyte concentration in solution was measured over time and experimental data then fit to the solution of Fick's second law [37,38]:

$$\frac{M_t}{M_\infty} = 1 - \frac{8}{\pi^2}\sum_{n=0}^{\infty} \frac{\exp\left[-\frac{D(2n+1)^2\pi^2 t}{L^2}\right]}{(2n+1)^2} \quad (1)$$

where M_t and M_∞ are the cumulative mass concentrations of the released molecule at time t and infinite time, respectively; L denotes the height of the cylindrical gel, and D is the diffusion coefficient of the molecule within the hydrogel. When $M_t/M_\infty \leq 0.6$, the early-time approximation can be used to calculate diffusivities according to [38]:

$$\frac{M_t}{M_\infty} = 4\left(\frac{Dt}{\pi L^2}\right)^{0.5} \quad (2)$$

For measurement of $\boldsymbol{D_{A,PEG}}$, acetate was loaded into the hydrogels by adding it to 300 μL of the hydrogel precursor solution at an acetate solution concentration of 1–1.1 M in a glass vial. The hydrogel precursor solution was then pipetted inside a 2 mL vial to form a cylindrical hydrogel of 6 mm height after gelation. 1.5 mL of ultrapure water was added to the vial, and the vial was incubated at room temperature. The

solution concentration of acetate was measured by sampling at 15 to 30 min intervals. At each time point, 2 μL solutions were removed for measurement of acetate concentration by measuring absorbance at 210 nm with a ThermoScientific NanoDrop 1000 Spectrophotometer. Equivalent volumes of fresh ultrapure water were added back to the solution during each sampling period to maintain constant volume throughout the experiment. Similarly, for measurement of $\mathbf{D_{N,PEG}}$, 300 μL of hydrogel precursor solution was pipetted inside a 2 mL vial to form a hydrogel of 6 mm height. After hydrogel formation, 1 mL of 1,500 mg N/L solution was pipetted into the vial and left for 48 h to reach equilibrium. Ammonium solution was then removed and replaced with ultrapure water. The solution concentration was sampled in 15 to 60 min intervals and each time was replaced with another 1 mL of ultrapure water. The concentration of ammonium was obtained using an ion chromatograph equipped with cation and anion columns and detectors (Dionex ICS 5000, Thermo Fisher Scientific, Waltham, MA). All diffusivity measurements were performed in triplicate for each condition.

The NH_4^+-N – hydrogel partition coefficient ($\boldsymbol{K_d}$), which is the ratio of the concentration of NH_4^+-N in the hydrogel to NH_4^+-N in solution at equilibrium, was also measured. 200 μL of precursor solution was prepared as described in Section 2.2 to generate PEGVS-PEGTT hydrogels in a 2 mL vial. 1 mL of ultrapure water was then pipetted onto the hydrogel for 24 h to allow for hydrogel swelling. After removing the ultrapure water, 500 μL of NH_4^+-N contacting solution at 10 g N/L was pipetted into the vials and allowed to equilibrate for 120 h. Both the initial (C_o) and equilibrium (C_e) NH_4^+-N concentrations in the contacting solution were measured in mg N/L using ammonium TNT plus Hach kits. $\boldsymbol{K_d}$ was calculated using the equation [39,40]:

$$K_d = \frac{(C_o - C_e)}{C_e} \bullet \frac{V_{sol}}{V_{hyd}} \tag{3}$$

where V_{sol} is the volume of the NH_4^+-N contacting and V_{hyd} is the volume of the swollen hydrogel. The experiment to measure $\boldsymbol{K_d}$ was performed in triplicate.

2.4. COMSOL Multiphysics modeling of mass transfer in hydrogels

COMSOL Multiphysics® (version 6.0) was used to model the mass transfer of acetate substrate throughout the hydrogel. The goal here was to identify hydrogel thicknesses, $\boldsymbol{L_{MAX}}$, defined as the thickness beyond which diffusion limitations inhibitory to the function of the ARB biofilm would occur for a range of metabolic consumption rates, $\boldsymbol{N_{ARB}}$ (1.6×10^{-6} to 12.8×10^{-5} mol/m^{2}s), obtained from literature [41,42]. The $\boldsymbol{N_{ARB}}$ values were used as a constant flux boundary condition in the COMSOL model at the biofilm-hydrogel interface. The transport of diluted species in porous media model in COMSOL was used with the following assumptions: (1) hydrogel deformation was negligible, (2) hydrogel degradation did not occur, (3) the ambient medium is infinite and well-stirred at all times, and thus, the concentration of the acetate was constant (40 mM) in the external media, (4) biofilm substrate consumption rate of acetate remained constant and was equivalent to the acetate flux at the biofilm-hydrogel interface, (5) no significant flux from the ends of the hydrogel. $\boldsymbol{L_{MAX}}$ for each metabolic consumption rate was determined by adjusting the hydrogel thickness until the acetate concentration at the biofilm-hydrogel interface was zero (i.e. acetate is instantly consumed by the biofilm, flux of acetate is diffusion limited).

2.5. MEC reactor setup and anode current generation

The biofilm anodes were developed in a two-chamber H-type reactor operated as a microbial electrolysis cell (MEC) to prevent oxygen diffusion that could inhibit microbial activity and to provide the optimum anode potential for maximizing ARB growth on the anode biofilm [43]. Two H-type reactors were used in the experiment, each containing an anode and a cathode compartment separated by an anion exchange membrane (AEM). The two compartments each held a volume of 585 mL. The anode compartment contained two rectangular graphite electrodes in the anode, with a total surface area of 33 cm^2, and the cathode compartment contained one 16 cm^2 rectangular electrode. The anode electrodes were maintained at a potential of −301 mV vs. a standard Ag/AgCl reference electrode. The reactors were kept in a temperature-controlled environment to maintain 30 °C conditions, while the anode compartment was mixed at a rate of 100 rpm.

The biofilm in each of the two reactors was established by adding anaerobic sludge obtained from the Salina Wastewater Treatment Plant (Salina, KS) to the anode. The sludge was added at a concentration of 1 % v/v to a phosphate buffer media containing the following composition per liter: 12.04 g Na_2HPO_4, 2.06 g KH_2PO_4, and 0.41 g NH_4Cl; 10 mL of a 1 L trace mineral media containing 0.5 g EDTA, 0.082 g $CoCl_2{\cdot}6H_2O$, 0.114 g $CaCl_2{\cdot}2H_2O$, 0.01 g H_3BO_3, 0.02 g $Na_2MoO_4{\cdot}2H_2O$, 0.001 g Na_2SeO_3, 0.01 g $Na_2WO_4{\cdot}2H_2O$, 0.02 g $NiCl_2{\cdot}6H_2O$, 1.16 g $MgCl_2$, 0.59 g $MnCl_2{\cdot}4H_2O$, 0.05 g $ZnCl_2$, 0.01 g $CuSO_4{\cdot}5H_2O$, and 0.01 g $AlK(SO_4)_2$; 1 mL of a 4 g/L $Fe(II)Cl_2$ stock solution; 0.5 mL of a 37.2 g/L $Na_2S{\cdot}9H_2O$ stock solution [44,45]. Acetate was then added as an electron donor to grow and condition the biofilm at a concentration of 40 mM. The cathode media was the same as the anode media, without the sludge or acetate, but was adjusted to a pH of 11.5 using sodium hydroxide. Once the biofilm began to grow on the anode electrodes, the media was replaced with the same composition described above, except the sludge. This was repeated until the reactor produced current densities of 5–8 A/m^2. Once the reactor had reached this stable point, one of the two electrodes present could be coated with the hydrogel. This novel design was developed so both anodes with or without the coating will be exposed to identical operating conditions in the same anode compartment, enabling a side-by-side comparison of performance. The electron donor concentrations were quantified by high-performance liquid chromatograph (HPLC) analysis (Shimadzu LC-20AT, USA) using an Aminex HPX-87H column (Bio-Rad Laboratories, USA) to separate the organic acids and sugars, which then were detected by a photodiode array and refractive index detectors. The current production from the reactors was continuously measured using a multichannel potentiostat (VMP3, Biologic, TN, USA), with current from both coated and uncoated electrodes in the same anode compared while being monitored separately.

2.6. Hydrogel-bioanode deposition procedure

A facile and reproducible method for depositing the hydrogel layer over an MEC anode was developed using a coating mold which was first fabricated by wrapping static tape (40 μm thick) around a plain electrode to a thickness of approximately 700–800 μm. Parafilm was then wrapped around the covered electrode and pressed onto another parafilm sheet to close the base (Fig. S2**A**). The tape-covered electrode was then gently pulled out of the parafilm mold, resulting in a hollow cuboid closed off at the base, and placed at the center of a petri dish. A second anode containing a biofilm was then centered in the mold, forming a gap between the anode biofilm and the mold. Coating of anodic biofilms with hydrogels was performed in an anaerobic chamber (Coy Labs, MI, USA). A hydrogel precursor solution was first prepared by adding 448 μL of PEGVS (49 mM) in water to 1,000 μL of phosphate buffer, pH 8. Then, 552 μL of PEGTT (20 mM) was added to the mixture to obtain an equimolar concentration of vinyl sulfone:thiol reactive groups, each at a final concentration of 22 mM and a total volume of 2,000 μL. A biofilm-functionalized anode was then placed in the center of the parafilm mold, and liquid hydrogel precursor solution was added to the mold until the gap was full (~1,500 μL) and allowed to react over the anode for 1 h at room temperature under vacuum. After gelation, the parafilm holder was gently unwrapped from the anode electrode, at which point the hydrogel was stabilized to the anode **(**Fig. S2**B)**.

2.7. Initial testing of coating impacts on current production and longevity of coating

Both the coated and uncoated electrodes were allowed to reach high current density in the MEC setup under copiotrophic conditions (acetate concentrations of 40 mM or higher). As previously described, the current production from each electrode was normalized to the 16 cm^2 area of each anode and compared. Two trials took place over a period of at least two weeks to assess the sustained attachment and longevity of the hydrogel coatings and to compare the performance of the coated and uncoated electrodes. A separate set of batch anode experiments was then conducted to evaluate the specific response of the coated and uncoated electrodes to very low levels of acetate concentrations in the media (2.5 mM) to mimic oligotrophic environments.

2.8. Ammonium spike experiments

After the batch experiments described above, stable current densities were allowed to sustain for the coated and uncoated electrodes with regular MEC media containing acetate as the electron donor. The current density response during this period served as the baseline for current density comparisons to the toxicant, NH_4^+-N. A shock load of ammonium chloride was added to yield a concentration of 10 g NH_4^+-N /L for the respective batch trials, mimicking concentrations that occur in relevant waste matrices. The biofilm response to the toxicant was monitored through current production for both the coated and uncoated electrodes over a time period of 1–4 days. The media in the anode compartments was replaced after this time with regular acetate media without NH_4^+-N and the recovery response for the two anodes was also monitored over a period of 1–4 days. The MECs were then returned to regular operation. Two trials of the ammonia spike experiments were performed.

3. Results and discussion

3.1. Hydrolytic stability of protective hydrogels

Hydrogels were formed by Michael addition reactions between vinyl sulfone and thiol end groups present on PEGVS and PEGTT precursor molecules (Fig. 1). These precursors create PEGVS-PEGTT hydrogels with an average 14 nm mesh size [46], and can be coated over ARB biofilms on anode substrates that are placed in the same compartment as uncoated substrates for side-by-side comparisons to reveal the impact of the coatings. Herein, hydrogel coated ARB biofilm electrodes are referred to as test anodes and uncoated ARB biofilm electrodes are referred as control anodes.

Prior to hydrogel coating over biofilm anodes, it was necessary to investigate the hydrolytic stability of PEGVS-PEGTT hydrogels. Bacteria were previously observed to cause degradation in similar PEGTT-PEGDA hydrogels during culture [25], likely by acidification of the local environment to cleave hydrolytically-liable ester linkages present between hydrogel crosslinks [47]. Because anodic biofilms generate H^+ during anaerobic oxidation of acetate or other substrates [48], a drop in pH within the local hydrogel environment was also expected here. This motivated a systematic study of PEGTT-PEGVS hydrolytic stability, with side-by-side comparison to hydrolytically-liable PEGTT-PEGDA hydrogels.

Hydrolytic stability was characterized by measuring swelling ratios during incubation in buffers across a range of pH values (pH 3–10). Increases in swelling ratios indicate degradation due to hydrolysis of chemical crosslinks, causing an influx of water into the hydrogel [49]. PEGVS-PEGTT hydrogels incubated at pH 3, pH 7, and pH 10 only reached 1.16, 1.08, and 1.18 times their initial mass, respectively, demonstrating minimal hydrogel degradation and long-term stability, which was confirmed by visual observations of intact PEGVS-PEGTT hydrogels at the end of the 72 day incubation period (**Fig. 2A and 2B**). In contrast, PEGTT-PEGDA control hydrogels were completely hydrolyzed and dissolved in solution within 24 h in pH 10 buffer. After 60 days, the PEGDA hydrogels in pH 3 and pH 7 reached 1.64 and 2.44 times their initial mass, indicating significant degradation of the hydrogel structure. A decrease in PEGDA-PEGTT hydrogel stiffness was also noted during visual observation (Fig. 2**A**), confirming that network degradation occurred in the control hydrogels. This set of observations agrees with literature that reports that the thioether-sulfone bonds present within PEGDA-PEGTT hydrogels are hydrolytically stable [34], and verifies that when used as a protective coating, the PEGDA-PEGTT hydrogel can accommodate a broad range of pH values possible in a waste stream [50,51], or from localized pH gradients across the anodic biofilm during MEC operation.

3.2. Acetate diffusion and hydrogel thickness

As the PEGDA-PEGTT hydrogels (herein referred to only as PEG hydrogels) provide a diffusive barrier to mass transport, it must be deposited over the bioanode at a thickness that allows for a flux of

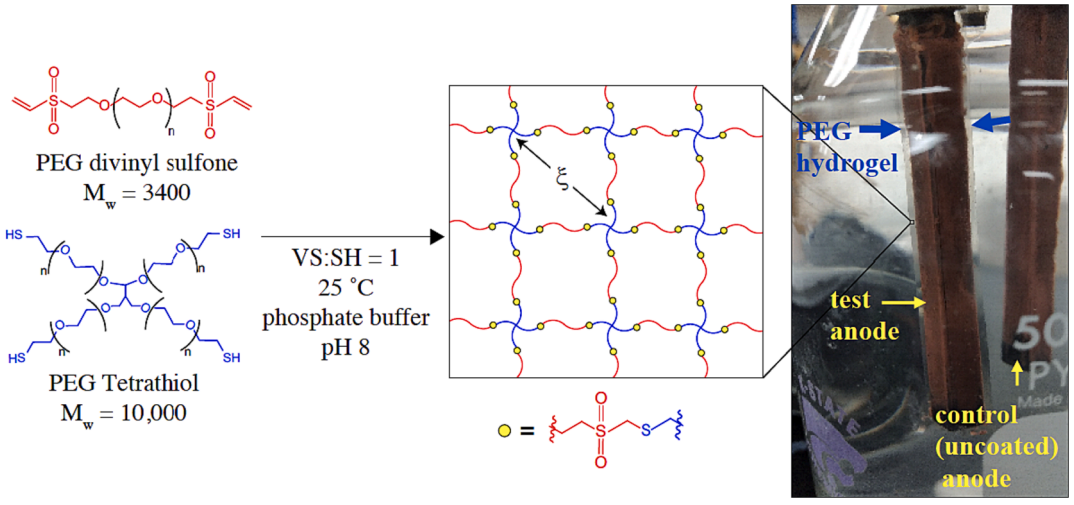

Fig. 1. PEGVS-PEGTT hydrogels as protective coatings for electroactive biofilms. PEGVS and PEGTT precursor molecules are mixed together at an equimolar thiol: vinylsulfone ratio over an electroactive biofilm on a test anode to generate a PEG hydrogel coating with thioether-sulfone crosslinks (yellow dots) and an average pore size of ξ = 14 nm. A control (uncoated) anode (background) is included in the same MEC chamber for side-by-side comparisons of current densities under identical chemical environments.

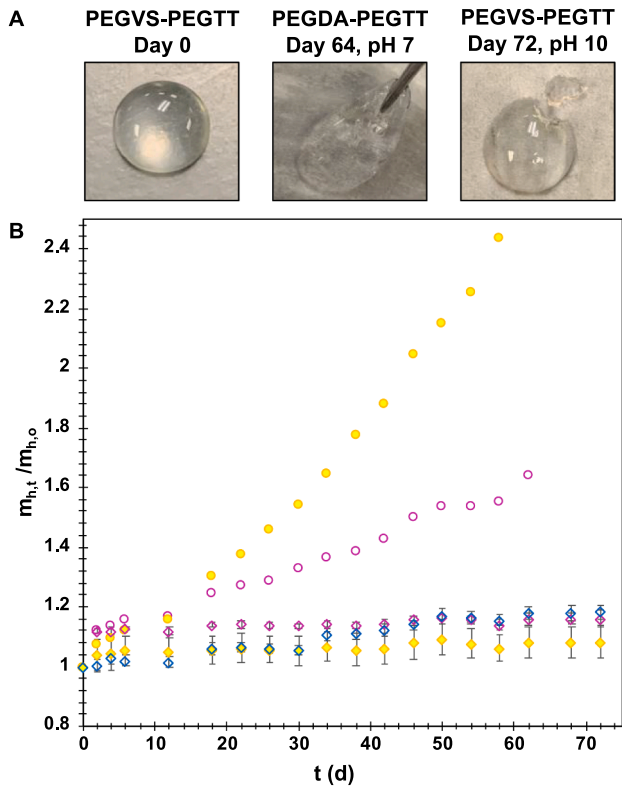

Fig. 2. Hydrolytic stability of PEGVS-PEGTT and PEGDA-PEGTT hydrogels. (A) Representative images of hydrogels before and after swelling experiments. (B) Swollen PEGVS-PEGTT and PEGDA-PEGTT hydrogel mass ($m_{h,t}$) relative to initial hydrogel mass ($m_{h,o}$) with time during incubation in buffers at pH 3, 7, and 10. Legend: pink circles = PEGDA-PEGTT, pH 3; yellow circles = PEGDA-PEGTT, pH 7; pink diamonds = PEGVS-PEGTT, pH 3; yellow diamonds = PEGVS-PEGTT, pH 7; blue diamonds = PEGVS-PEGTT, pH 10.

nutrient (acetate) that can support the metabolic demands of ARB biofilms at the hydrogel-biofilm interface. To understand the effect of hydrogel thickness on acetate flux to the biofilm interface, it was first necessary to estimate the diffusion coefficient of acetate through the coatings ($D_{A,PEG}$), as hydrogels can hinder the diffusive transport of solute molecules through hydrogen bonding, electrostatic interactions, and van der Waals forces between solutes and PEG chains [52]. The release profile of acetate from PEG hydrogels was plotted according to the mass fraction of acetate released with time (Fig. 3**A**). Using Fick's law for early release time (Fig. 3**A, inset**), $D_{A,PEG}$ was calculated to be 1.44×10^{-10} m^2/s, an 87 % decrease relative to acetate diffusivity in water [53], and a diffusivity comparable to other small molecules such as glucose through similar PEG hydrogels (1.29×10^{-10} m^2/s [54]).

With determination of $D_{A,PEG}$, finite element modeling was used to estimate the concentration profile and flux of acetate throughout the hydrogel coating. Using an acetate solution concentration of 40 mM and a biofilm metabolic consumption (N_{ARB}) rate of 6.4×10^{-6} mol/m^2s, a steady state concentration profile of acetate throughout the hydrogel was obtained, with an acetate concentration of 0.094 mM determined at the biofilm-hydrogel interface (Fig. 3**B**). With the working model, the maximum hydrogel thickness (L_{MAX}) that could be present over the biofilm while still enabling an acetate flux meeting the full metabolic requirements of a biofilm (i.e. without creating diffusion limitations) was estimated, given the model assumptions listed in Section 2.4. Simulation was conducted with N_{ARB} values ranging between 1.6×10^{-6} and 12.8×10^{-5} mol/m^2s, corresponding to acetate consumption rates of young to mature ARB biofilms [41,42]. This provided an understanding of the conditions at the biofilm-hydrogel interface and guidance for film coating deposition thicknesses compatible with ARB biofilms. As

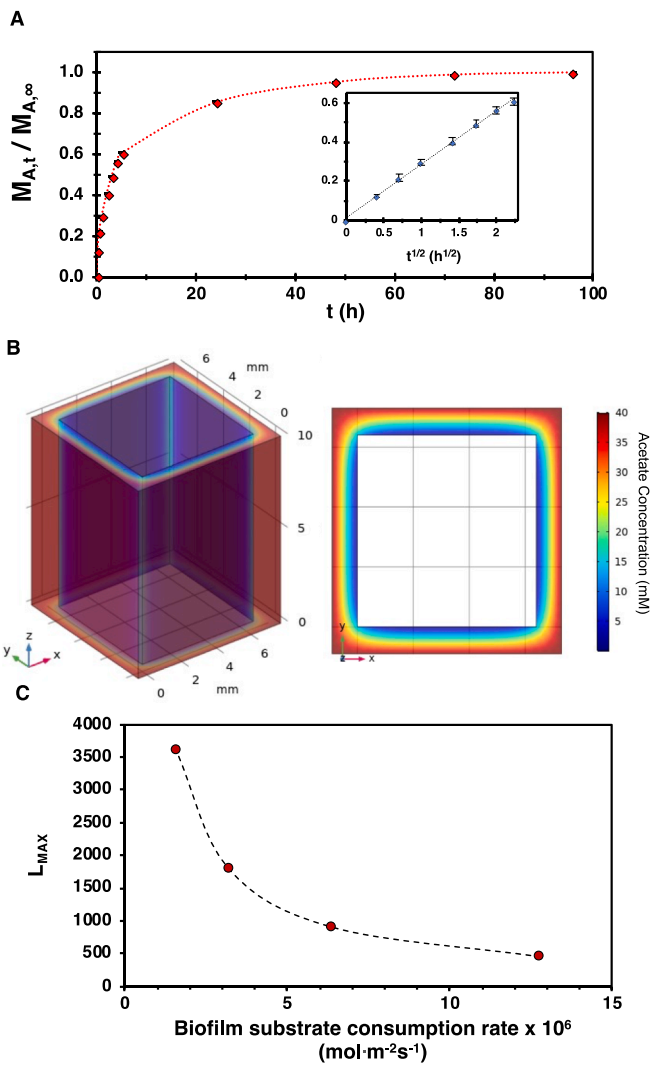

Fig. 3. (A) Release kinetics of acetate from PEG hydrogels to determine $D_{A,PEG}$. (Inset) Early time ($M_{A,t}/M_{A,\infty} < 0.6$) release used for $D_{A,PEG}$ quantification according to Equation (2). (B) COMSOL simulation results of acetate concentrations (mM) throughout the PEG hydrogel coating layer. (C) L_{MAX} values at varied biofilm consumption rates of acetate.

expected, biofilms with higher metabolic demands had lower L_{MAX} values (Fig. 3**C**); as an example, a mature biofilm (N_{ARB} = 6.4×10^{-6} mol/m^2s [41,42]) would become diffusion limited when hydrogel thicknesses exceeded 900 μm. After swelling, hydrogels deposited over the anodes using the developed deposition procedure appeared ~ 2600 μm thick (Fig. S2**C**), corresponding to a N_{ARB} of ~ 2.3×10^{-6} mol/m^2s.

3.3. Impact of the hydrogel coatings on anode respiring bacteria

Biofilms were developed on both test and control electrodes to a stable and high current density (5–8 A/m^2) for duplicate batch experiments under copiotrophic conditions. These initial current densities were in line with high current density biofilms fed with acetate as an electron donor [43,55,56]. After coating, hydrogels appeared physically stable over ARB biofilms after swelling (Fig. 1), and these test anodes had an average decrease in current density of 40–50 % relative to the control anodes in both trials 1 and 2 (Fig. 4**A and 4B**). The drop can be attributed to the hindered diffusivity of acetate through the hydrogel coating with a thickness (~2600 μm) that likely exceeded the L_{MAX} for the biofilm present (Fig. 3**C**), creating a diffusion-limited environment where current density is dependent on the flux of acetate to the biofilm

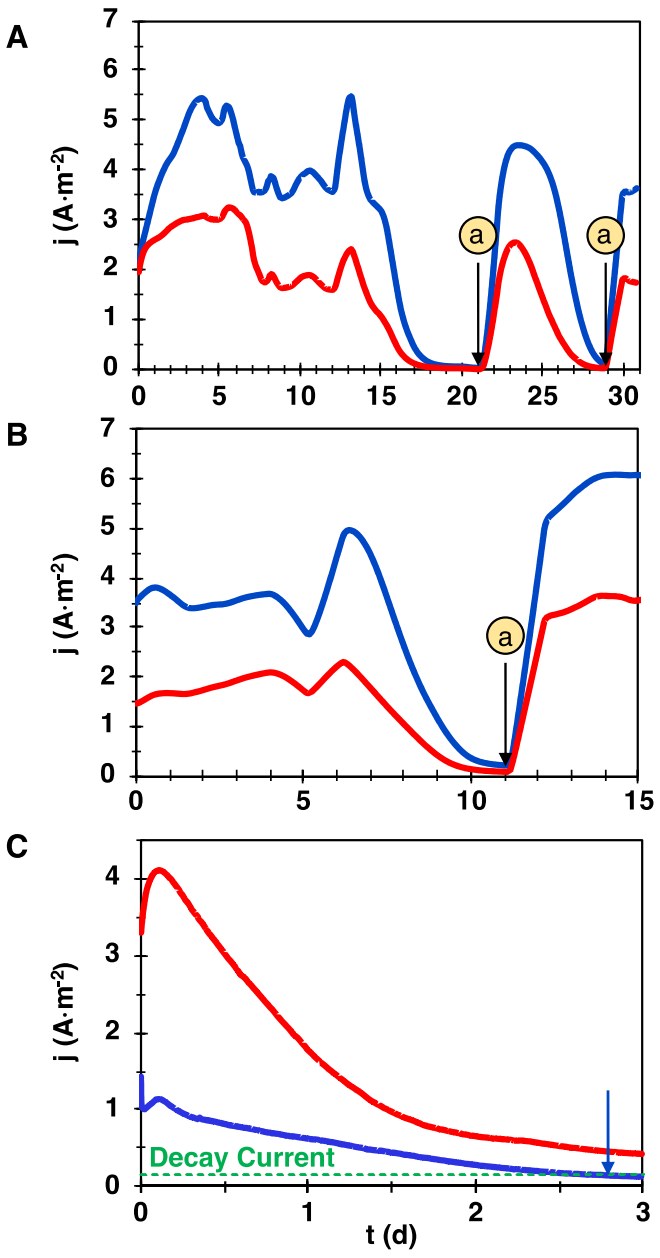

Fig. 4. Current densities (j) with time for the test anode (red) and control anode (blue) within the same electrode compartment under copiotrophic conditions (40 mM acetate) for (A) trial 1 and (B) trial 2. The arrows labeled with (a) represent acetate spikes added after acetate depletion. (C) Current densities (j) with time for the coated and uncoated anodes under oligotrophic conditions (2.5 mM acetate). Green line indicates decay current (0.14 A/m^2 which is typical for anode biofilm densities of 1.570 g VSS_{ARB}/m^2), blue arrow indicates the time that the control anode drops below the decay current.

as opposed to the maximum metabolic consumption rate of the biofilm. The drop could be further attributed to a lower diffusivity of phosphate buffer through the hydrogel coating, as phosphate transport into the biofilm was previously shown to be a critical determinant of current density [48]. Despite the noted decrease, test anodes showed stable and sustained current densities over a one month time period and it mimicked the responses of the control anode during perturbations in acetate levels (Fig. 4**A and 4B**). No visible signs of hydrogel detachment or loss in biofilm viability were noted at the end of each trial. This demonstrates hydrogel longevity, in line with its hydrolytic stability previously observed (Fig. 2**B**). The long-term (15–30 day) biocompatability of the hydrogel with ARB biofilms can also be observed by tracking the difference in current densities between the control and test anodes. The current density difference fluctuates between 0 and 3 A/m^2, depending on transient electron donor (acetate) levels, however the difference did not have an increasing trend with time in either trial (**Fig. S3**). This indicates that although the hydrogel coatings did not enhance biofilm activity, it did not compromise its activity beyond the initial drop. It is also important to note that the primary aim of the coatings was to protect the anode biofilm from environmental stressors and not to enhance current density, which could be increased by adding conductive nanomaterials into the hydrogel, as others have demonstrated [9,13–16].

After operation under copiotrophic conditions, test and control anodes were exposed to an oligotrophic environment with low acetate concentration (2.5 mM or 160 mg COD/L). Both anodes responded with drops in current density (Fig. 4**C**), consistent with previous findings that ARB opt to shut down or slow their electroactive metabolism on anode surfaces under severe electron donor or acceptor limitations [57–59]. Despite this drop, the test anode initially produced a significantly higher current density of over 3 A/m^2, followed by a decreasing current density in response to the low acetate availability. This was in contrast to the uncoated anode, which responded with a more dramatic drop in initial current density to 1.2 A/m^2 with a steady decline thereafter. During the latter part of the experiment, the test anode sustained a higher current density of ~ 0.4 A/m^2 for more than 24 h compared to the control anode, which sustained a 4 × lower current density of ~ 0.1 A/m^2 for the same duration. Importantly, the hydrogel coating kept the test anode above the decay current (0.14 A/m^2) that corresponds to biomass decay at typical anode biomass concentrations of ~ 1.57 g VSS_{ARB}/cm^2 (VSS_{ARB} = active biomass concentration of anode respiring bacteria on the anode surface) and not due to oxidation of a substrate (acetate) [60]. By contrast, current density from the uncoated control anode dropped below the decay current after 2.8 days. This highlights the positive impact of the hydrogel coatings in promoting biofilm survival in environments with low organic content, a condition relevant to environments where MxCs are finding emerging applications in, such as marine and sediment ecosystems [61]. The differing responses between the two anodes was likely due to the fact that under starved conditions, the biofilm on the test anode was protected from cell loss to the bulk liquid. Instead, ARB remained encapsulated within the hydrogel, enabling the biofilm to maintain its metabolic activity. In contrast, ARB in uncoated biofilms under starvation, which are also directly exposed to fluid shear, are lost to the bulk fluid causing the control anodes to become more vulnerable to compromised biofilm activity. Furthermore, the constrained acetate and buffer transport through the coating acclimatized the biofilm on the test anode to survival under limited substrate availability, a behavior that has been regularly evidenced in anaerobic ecosystems, including anodic biofilms [62].

3.4. *Characterization of PEG - NH_4^+-N chemical interactions*

To assess the impact of the hydrogel on the biofilm during NH_4^+-N exposure, chemical interaction parameters between NH_4^+-N and PEG hydrogels were first characterized. Specifically, the partition coefficient ($\boldsymbol{K_d}$) and the diffusivity of NH_4^+-N through PEG hydrogel ($\boldsymbol{D_{N,PEG}}$) were measured. A $\boldsymbol{K_d}$ value of 0.94 ± 0.08 was quantified, suggesting that NH_4^+-N was only slightly favored in bulk solution. However, quantification of $\boldsymbol{D_{N,PEG}}$ using the NH_4^+-N release profile from PEG hydrogels (Fig. 5**)** revealed that NH_4^+-N diffusion was significantly hindered. Here, $\boldsymbol{D_{N,PEG}}$ was found to be 1.88x10^{-6} cm^2/s, representing a 90 % decrease in diffusivity compared to NH_4^+-N in water at the same temperature ($\boldsymbol{D_{N,WATER}}$ = 1.81x10^{-5} cm^2/s [63]).

To our knowledge, this is the first report of $\boldsymbol{K_D}$ and $\boldsymbol{D}$ for NH_4^+-N in PEG hydrogels. The results indicate that hindered transport of NH_4^+-N to the biofilm is a key feature of the protective hydrogel coatings. With this finding, it was hypothesized that the coatings could provide benefits to

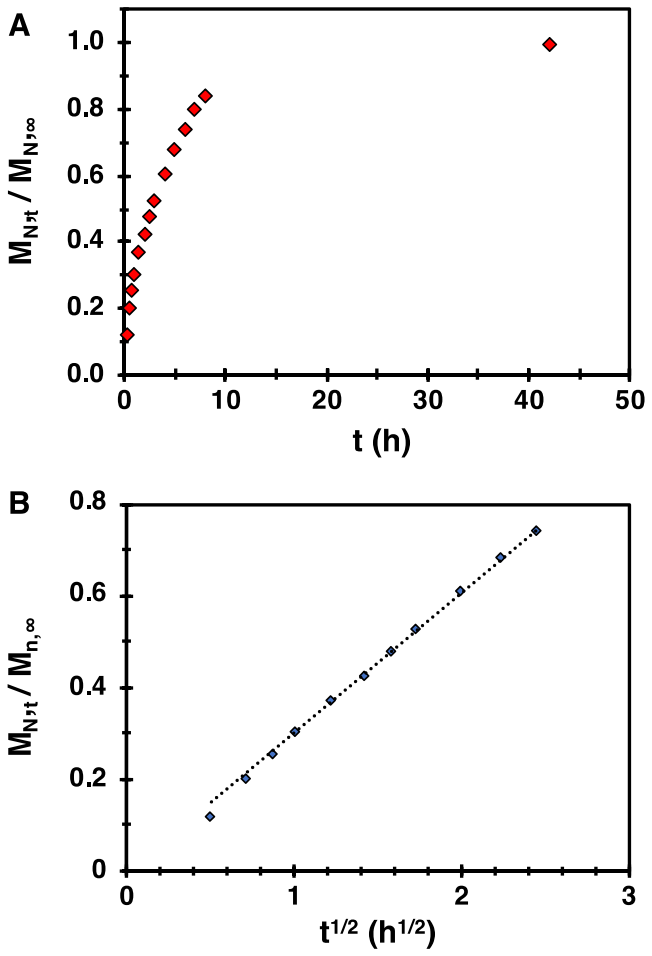

Fig. 5. (A) Release kinetics of NH_4^+-N from PEG hydrogels after NH_4^+-N was loaded into hydrogels at an initial concentration of 1500 mg/L. (B) Early time ($M_{N,t}/M_{N,\infty} < 0.6$) release profile used to determine $\boldsymbol{D_{N,PEG}}$ using Equation (2).

the biofilm during transient periods of exposure to high concentrations of NH_4^+-N (i.e. NH_4^+-N shocks), as can occur in industrial and municipal wastewaters [64]. This hypothesis was tested in the next section.

3.5. Protection of anode biofilm against ammonia shock from hydrogel coatings

To evaluate the ability of PEG coatings to protect anode biofilms from NH_4^+-N shocks, test and control anodes were exposed to 10 g/L NH_4^+-N for one day, and two replicate trials were performed at different time points. The anodes were first subjected to baseline operation conditions (40 mM acetate) to achieve a pre–shock baseline (Fig. 6, pre-shock). In both trials, test anodes displayed a 1–1.5 A/m^2 decrease in current density compared to the control, consistent with the differences observed in Section 3.3. On NH_4^+-N exposure (Fig. 6, NH_4^+-N shock), an initial decrease in absolute current densities was evident in both test and control anodes. During the following 2–6 hours of the shock, a difference in response to high NH_4^+-N levels between the control and test anodes was noted. Control anodes showed an initial spurt in current density, likely due to the pH-dependent response of the biofilm anode that precedes the impact of toxicity on the ARB. Here NH_4^+-N together with phosphate buffer can facilitate proton transport to enable ARB to overcome pH inhibition. High concentrations of NH_4^+-N can also be initially counteracted by anaerobic bacteria through alternate ion transport mechanisms, per the noncompetitive inhibition model [8,65,66]. However, this effect was short-lived on the control anodes, as the metabolic toxicity of NH_4^+-N on the uncoated ARB biofilms quickly outcompeted the positive impact from pH buffering and proton transport, as noted by the sharp decrease in control anode current density after the initial rise. While the test anodes also showed decreasing current densities, within ~ 6 hours of the shock period, the positive impact of the hydrogel could be observed in both trials. By this time, current densities in the test anodes surpassed those of the control anodes. After 1 day of NH_4^+-N exposure, the test anodes achieved a stabilized current density of about 15–30 % higher than the control anodes. This was likely due to the lower value of $\boldsymbol{D_{N,PEG}}$ relative to $\boldsymbol{D_{N,WATER}}$, which reduced the sharp chemical gradient and the effective NH_4^+-N concentration at the hydrogel-biofilm interface of the test anode, lowering biofilm exposure to the toxicant over the shock period.

After the NH_4^+-N shock, regular acetate media was re-introduced to the anode compartment. During the following 24–36 hours of this post-shock period, test anodes in both trials produced higher current densities and returned to the pre-shock current densities faster than the control anodes (Fig. 6, post-shock). This improved response can be attributed to inhibited NH_4^+-N transport through the coatings, resulting in a lower overall exposure to NH_4^+-N at the hydrogel-biofilm interface during the NH_4^+-N shock, rendering healthier biofilms and faster biofilm recovery. After 3–4 days, the current density in the control anodes also reverted back to pre-shock conditions, indicating that both coated and uncoated biofilms were able to make a full recovery from the NH_4^+-N shock. Taken together, the higher current densities of the test anodes during the NH_4^+-N shock, combined with its faster recovery afterwards, is of particular significance because of its relevance in industrial and municipal wastewaters, where cyclic patterns of high toxin exposure can occur [64].

4. Outlook and future recommendations

The results demonstrate that PEG hydrogel coatings on MxC anodes can benefit electrochemical biofilm systems that become exposed to sharp chemical gradients, common in MxCs carrying out nitrification and fermentation [67], or those that must function under low nutrient environments. Beyond ammonia exposure, hydrogel coatings may be further developed to protect against other inhibitory compounds such as dissolved oxygen, H_2S, perchlorate, peroxides, and other toxins, particularly when catalytic materials (e.g. enzymes [22,68] or nanoparticles [69]) can be added to the hydrogel to facilitate the selective degradation of these compounds before they reach the biofilm. The sustained, higher net current densities from hydrogel coated anodes under oligotrophic environments can also facilitate MxC operation in new environments, such as municipal wastewater, sub-surface groundwater, soil, and marine environments. Combined with the well-known anti-fouling characteristics of PEG [23], these hydrogel coatings may enable MxC application in ocean beds for self-powered, underwater biobatteries [61], for example. Improved computational models that couple mass transport within hydrogel coatings with spatial and temporal aspects of ARB biofilm function in these dynamic environments will be necessary to guide the further design and development of these protective coatings for the aforementioned applications.

Beyond MxCs, the coatings are applicable to protection of conventional (non-electrochemical) biofilm systems in water/wastewater treatment and nutrient removal processes that rely on granulated sludge-based technologies such as ANAMMOX, AQUA – NEREDA [70,71] by impeding the exposure of the granules to high toxicant concentrations. Membrane Biofilm Reactors (MBfRs) that often involve sequential or concomitant removal of multiple contaminants in groundwater may also benefit from hydrogel coated biofilms [72]. The hydrogel coating can provide tunable diffusive transport control of the contaminants into the MBfR biofilm, thereby providing additional flexibility for removal mechanisms to achieve superior multi-component removals. Detailed studies and feasibility analyses of hydrogel coatings will need to be carried out for each of these areas for successful application.

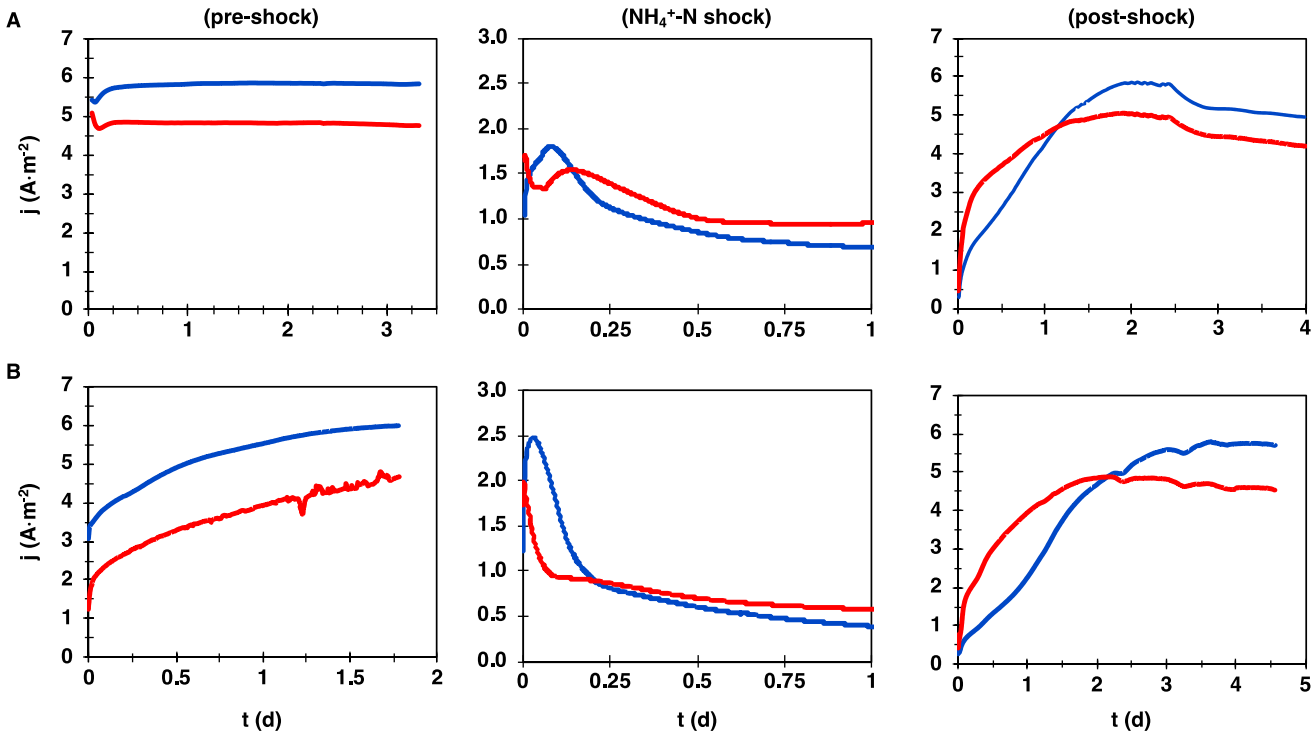

Fig. 6. Current density (j) response of the test (red) and control (blue) anodes with the addition of a toxic load of NH_4^+-N (10 g/L) during two replicate trials, trial 1 **(A)** and trial 2 **(B)**. Current densities during pre-shock, NH_4^+-N shock, and post-shock time periods are shown.

5. Conclusion

This study is significant as it provides a novel demonstration of protective PEG hydrogel coatings applied on a highly functional MxC anode, where performance was compared side-by-side to a co-located, uncoated anode biofilm. Hydrogel coated biofilm anodes provided sustained electroactivity with current densities that were reduced but comparable to control anodes under copiotrophic conditions, while providing a 4× higher current density for a sustained duration under oligotrophic conditions. Exposure of the anodes to NH_4^+-N shocks revealed that the coatings had a favorable impact on biofilm viability, as indicated by higher current densities on test anodes compared to the control anodes during the shock, and faster biofilm recovery after the shock.

Author contributions

NF, JR, EH, PF, RH, and PP conceived and designed experiments. NF, JR, EH, PF performed experiments. NF, JR, EH, RH, and PP wrote the manuscript. All authors have approved of the submitted version of the manuscript.

Declaration of Competing Interest

The authors declare that they have no known competing financial interests or personal relationships that could have appeared to influence the work reported in this paper.

Data availability

Data will be made available on request.

Acknowledgements

We acknowledge NSF Award #1841613 for support of this work. NF, JR, and EH would also like to acknowledge the KSU R^3 graduate program supported through the NRT-INFEWS program (NSF Award #1828571). We acknowledge the Kansas State University Game Changing Research Initiation Program (KGRIP) seed award for its support.

Appendix A. Supplementary data

Supplementary data to this article can be found online at https://doi.org/10.1016/j.bioelechem.2023.108595.

References

[1] S.C. Popat, C.I. Torres, Critical transport rates that limit the performance of microbial electrochemistry technologies, Bioresour. Technol. 215 (2016/09/01/ 2016,) 265–273, https://doi.org/10.1016/j.biortech.2016.04.136.
[2] B.E. Logan, K. Rabaey, Conversion of Wastes into Bioelectricity and Chemicals by Using Microbial Electrochemical Technologies, Science 337 (6095) (2012) 686–690, https://doi.org/10.1126/science.1217412.
[3] T.H.J.A. Sleutels, A. Ter Heijne, C.J.N. Buisman, H.V.M. Hamelers, Bioelectrochemical Systems: An Outlook for Practical Applications, ChemSusChem 5 (6) (2012) 1012–1019, https://doi.org/10.1002/cssc.201100732.
[4] A.P. Borole, G. Reguera, B. Ringeisen, Z.-W. Wang, Y. Feng, B.H. Kim, Electroactive biofilms: Current status and future research needs, Energy Environ. Sci. 4 (12) (2011) 4813.
[5] A. Milbrandt, T. Seiple, D. Heimiller, R. Skaggs, A. Coleman, Wet waste-to-energy resources in the United States, Resour. Conserv. Recycl. 137 (2018/10/01/ 2018,) 32–47, https://doi.org/10.1016/j.resconrec.2018.05.023.
[6] P. Cheung, "Anaerobic digestion on swine manure: inhibition by ammonia and hydrogen sulfide," Ph.D., School of Engineering, University of Guelph, 2004. [Online]. Available: https://hdl.handle.net/10214/20318.
[7] K.H. Hansen, I. Angelidaki, B.K. Ahring, ANAEROBIC DIGESTION OF SWINE MANURE: INHIBITION BY AMMONIA, Water Res. 32 (1) (1998/01/01/ 1998,) 5–12, https://doi.org/10.1016/S0043-1354(97)00201-7.
[8] M. Mahmoud, P. Parameswaran, C.I. Torres, B.E. Rittmann, Electrochemical techniques reveal that total ammonium stress increases electron flow to anode respiration in mixed-species bacterial anode biofilms, Biotechnol. Bioeng. 114 (6) (2017) 1151–1159, https://doi.org/10.1002/bit.26246.
[9] X.-W. Liu, Y.-X. Huang, X.-F. Sun, G.-P. Sheng, F. Zhao, S.-G. Wang, H.-Q. Yu, Conductive carbon nanotube hydrogel as a bioanode for enhanced microbial electrocatalysis, ACS Appl Mater Interfaces 6 (11) (2014) 8158–8164.
[10] P. Kaiser, S. Reich, D. Leykam, M. Willert-Porada, A. Greiner, R. Freitag, Electrogenic Single-Species Biocomposites as Anodes for Microbial Fuel Cells, Macromol. Biosci. 17 (7) (2017).

[11] X. Tang, H.Y. Ng, Anthraquinone-2-sulfonate immobilized to conductive polypyrrole hydrogel as a bioanode to enhance power production in microbial fuel cell, Bioresour Technol 244 (Pt 1) (Nov 2017) 452–455, https://doi.org/10.1016/j.biortech.2017.07.189.
[12] S. Y. Lee *et al.*, "Bioelectricity Generation by Corynebacterium glutamicum with Redox-Hydrogel-Modified Carbon Electrode," *Applied Sciences,* vol. 9, no. 20, 2019, doi: 10.3390/app9204251.
[13] A. Szollosi, A. Hoschke, J.M. Rezessy-Szabo, E. Bujna, S. Kun, Q.D. Nguyen, Formation of novel hydrogel bio-anode by immobilization of biocatalyst in alginate/polyaniline/titanium-dioxide/graphite composites and its electrical performance, Chemosphere 174 (May 2017) 58–65, https://doi.org/10.1016/j.chemosphere.2017.01.095.
[14] J.Y. Chen, P. Xie, Z.P. Zhang, Reduced graphene oxide/polyacrylamide composite hydrogel scaffold as biocompatible anode for microbial fuel cell, Chem. Eng. J. 361 (2019) 615–624, https://doi.org/10.1016/j.cej.2018.12.116.
[15] G.G. Kumar, S. Hashmi, C. Karthikeyan, A. GhavamiNejad, M. Vatankhah-Varnoosfaderani, F.J. Stadler, Graphene oxide/carbon nanotube composite hydrogels-versatile materials for microbial fuel cell applications, Macromol Rapid Commun 35 (21) (Nov 2014) 1861–1865, https://doi.org/10.1002/marc.201400332.
[16] S.K. Suravaram, D.K. Smith, A. Parkin, V. Chechik, Conductive Gels Based on Modified Agarose Embedded with Gold Nanoparticles and their Application as a Conducting Support for Shewanella Oneidensis MR-1, ChemElectroChem 6 (23) (2019) 5876–5879, https://doi.org/10.1002/celc.201901618.
[17] Q. Du, T. Li, N. Li, X. Wang, Protection of Electroactive Biofilm from Extreme Acid Shock by Polydopamine Encapsulation, Environ. Sci. Technol. Lett. 4 (8) (2017) 345–349, https://doi.org/10.1021/acs.estlett.7b00242.
[18] H. Luo, S. Yu, G. Liu, R. Zhang, W. Teng, Effect of in-situ immobilized anode on performance of the microbial fuel cell with high concentration of sodium acetate, Fuel 182 (2016) 732–739, https://doi.org/10.1016/j.fuel.2016.06.032.
[19] M. Li, K. Lv, S. Wu, S. Chen, Immobilization of Anodophilic Biofilms for Use in Aerotolerant Bioanodes of Microbial Fuel Cells, ACS Appl Mater Interfaces 8 (51) (2016) 34985–34990, https://doi.org/10.1021/acsami.6b11064.
[20] M.J. Webber, E.T. Pashuck, (Macro)molecular self-assembly for hydrogel drug delivery, Adv. Drug Deliv. Rev. 172 (2021/05/01/ 2021,) 275–295, https://doi.org/10.1016/j.addr.2021.01.006.
[21] S.R. Caliari, J.A. Burdick, A practical guide to hydrogels for cell culture, Nat Methods 13 (5) (2016) 405–414, https://doi.org/10.1038/nmeth.3839.
[22] J. Dai, H. Zhang, C. Huang, Z. Chen, A. Han, A Gel-Based Separation-Free Point-of-Care Device for Whole Blood Glucose Detection, Anal Chem 92 (24) (2020) 16122–16129, https://doi.org/10.1021/acs.analchem.0c03801.
[23] P. Lundberg, A. Bruin, J.W. Klijnstra, A.M. Nyström, M. Johansson, M. Malkoch, A. Hult, Poly(ethylene glycol)-based thiol-ene hydrogel coatings-curing chemistry, aqueous stability, and potential marine antifouling applications, ACS Appl Mater Interfaces 2 (3) (2010) 903–912.
[24] K.W. Kolewe, J. Zhu, N.R. Mako, S.S. Nonnenmann, J.D. Schiffman, Bacterial Adhesion Is Affected by the Thickness and Stiffness of Poly(ethylene glycol) Hydrogels, ACS Appl Mater Interfaces 10 (3) (2018) 2275–2281, https://doi.org/10.1021/acsami.7b12145.
[25] A.J. van der Vlies, N. Barua, P.A. Nieves-Otero, T.G. Platt, R.R. Hansen, On Demand Release and Retrieval of Bacteria from Microwell Arrays Using Photodegradable Hydrogel Membranes, Acs Appl Bio Mater 2 (1) (2019) 266–276, https://doi.org/10.1021/acsabm.8b00592.
[26] N. Fattahi, P.A. Nieves-Otero, M. Masigol, A.J. van der Vlies, R.S. Jensen, R. R. Hansen, T.G. Platt, Photodegradable Hydrogels for Rapid Screening, Isolation, and Genetic Characterization of Bacteria with Rare Phenotypes, Biomacromolecules 21 (8) (2020) 3140–3151.
[27] N. Barua *et al.*, "Simultaneous Discovery of Positive and Negative Interactions Among Rhizosphere Bacteria Using Microwell Recovery Arrays," *Front Microbiol,* vol. 11, p. 601788, Jan 5 2021, doi: 10.3389/fmicb.2020.601788.
[28] N. Fattahi, N. Barua, A. J. van der Vlies, and R. R. Hansen, "Photodegradable Hydrogel Interfaces for Bacteria Screening, Selection, and Isolation," *JoVE,* vol. 177, p. e63048, 2021/11/04/ 2021, doi: 10.3791/63048.
[29] N. Barua, K. M. Clouse, D. A. Ruiz Diaz, M. R. Wagner, T. G. Platt, and R. R. Hansen, "Screening the maize rhizobiome for consortia that improve Azospirillum brasilense root colonization and plant growth outcomes," *Frontiers in Sustainable Food Systems,* vol. 7, 2023, doi: 10.3389/fsufs.2023.1106528.
[30] M. Masigol, E.L. Radaha, A.D. Kannan, A.G. Salberg, N. Fattahi, P. Parameswaran, R.R. Hansen, Polymer Surface Dissection for Correlated Microscopic and Compositional Analysis of Bacterial Aggregates during Membrane Biofouling, Acs Appl Bio Mater 5 (1) (2022) 134–145.
[31] P. van de Wetering, A.T. Metters, R.G. Schoenmakers, J.A. Hubbell, Poly(ethylene glycol) hydrogels formed by conjugate addition with controllable swelling, degradation, and release of pharmaceutically active proteins, J Control Release 102 (3) (2005) 619–627, https://doi.org/10.1016/j.jconrel.2004.10.029.
[32] S. Chatani, D.P. Nair, C.N. Bowman, Relative reactivity and selectivity of vinyl sulfones and acrylates towards the thiol–Michael addition reaction and polymerization, Polym. Chem. 4 (4) (2013) 1048–1055.
[33] P.M. Kharkar, M.S. Rehmann, K.M. Skeens, E. Maverakis, A.M. Kloxin, Thiol–ene Click Hydrogels for Therapeutic Delivery, ACS Biomater Sci. Eng. 2 (2) (2016/02/08 2016,) 165–179, https://doi.org/10.1021/acsbiomaterials.5b00420.
[34] D.P. Nair, M. Podgórski, S. Chatani, T. Gong, W. Xi, C.R. Fenoli, C.N. Bowman, The Thiol-Michael Addition Click Reaction: A Powerful and Widely Used Tool in Materials Chemistry, Chem. Mater. 26 (1) (2014) 724–744.
[35] J.I. Paez, A. Farrukh, R. Valbuena-Mendoza, M.K. Włodarczyk-Biegun, A. del Campo, Thiol-Methylsulfone-Based Hydrogels for 3D Cell Encapsulation, ACS Appl. Mater. Interfaces 12 (7) (2020/02/19 2020,) 8062–8072, https://doi.org/10.1021/acsami.0c00709.
[36] M.B. Browning, S.N. Cereceres, P.T. Luong, E.M. Cosgriff-Hernandez, Determination of the in vivo degradation mechanism of PEGDA hydrogels, J. Biomed. Mater. Res. A 102 (12) (2014) 4244–4251, https://doi.org/10.1002/jbm.a.35096.
[37] R. Takahashi, S. Sato, T. Sodesawa, and Y. Kamomae, "Measurement of the diffusion coefficient of nickel nitrate in wet silica gel using UV/VIS spectroscope equipped with a flow cell," *Physical Chemistry Chemical Physics,* 10.1039/A909375C vol. 2, no. 6, pp. 1199-1204, 2000, doi: 10.1039/A909375C.
[38] J. Siepmann, F. Siepmann, Modeling of diffusion controlled drug delivery, J. Control. Release 161 (2) (2012/07/20/ 2012,) 351–362, https://doi.org/10.1016/j.jconrel.2011.10.006.
[39] B. Semmling, S. Nagel, K. Sternberg, W. Weitschies, A. Seidlitz, Impact of different tissue-simulating hydrogel compartments on in vitro release and distribution from drug-eluting stents, Eur J Pharm Biopharm 87 (3) (Aug 2014) 570–578, https://doi.org/10.1016/j.ejpb.2014.04.010.
[40] A.F.R. Pimenta, J. Ascenso, J.C.S. Fernandes, R. Colaco, A.P. Serro, B. Saramago, Controlled drug release from hydrogels for contact lenses: Drug partitioning and diffusion, Int J Pharm 515 (1–2) (2016) 467–475, https://doi.org/10.1016/j.ijpharm.2016.10.047.
[41] H.-S. Lee, C.I. Torres, B.E. Rittmann, Effects of Substrate Diffusion and Anode Potential on Kinetic Parameters for Anode-Respiring Bacteria, Environmental Science & Technology 43 (19) (2009/10/01 2009,) 7571–7577, https://doi.org/10.1021/es9015519.
[42] P. Parameswaran, C.I. Torres, D.-W. Kang, B.E. Rittmann, R. Krajmalnik-Brown, The role of homoacetogenic bacteria as efficient hydrogen scavengers in microbial electrochemical cells (MXCs), Water Sci. Technol. 65 (1) (2012) 1–6, https://doi.org/10.2166/wst.2011.519.
[43] C.I. Torres, R. Krajmalnik-Brown, P. Parameswaran, A.K. Marcus, G. Wanger, Y. A. Gorby, B.E. Rittmann, Selecting Anode-Respiring Bacteria Based on Anode Potential: Phylogenetic, Electrochemical, and Microscopic Characterization, Environ. Sci. Tech. 43 (24) (2009) 9519–9524.
[44] P. Parameswaran, C.I. Torres, H.-S. Lee, R. Krajmalnik-Brown, B.E. Rittmann, Syntrophic interactions among anode respiring bacteria (ARB) and Non-ARB in a biofilm anode: electron balances, Biotechnol. Bioeng. 103 (3) (2009) 513–523, https://doi.org/10.1002/bit.22267.
[45] P. Parameswaran, C.I. Torres, H.-S. Lee, B.E. Rittmann, R. Krajmalnik-Brown, Hydrogen consumption in microbial electrochemical systems (MXCs): The role of homo-acetogenic bacteria, Bioresour. Technol. 102 (1) (2011/01/01/ 2011,) 263–271, https://doi.org/10.1016/j.biortech.2010.03.133.
[46] S.P. Zustiak, J.B. Leach, Hydrolytically Degradable Poly(Ethylene Glycol) Hydrogel Scaffolds with Tunable Degradation and Mechanical Properties, Biomacromolecules 11 (5) (2010/05/10 2010,) 1348–1357, https://doi.org/10.1021/bm100137q.
[47] C. Hiemstra, L.J. van der Aa, Z. Zhong, P.J. Dijkstra, J. Feijen, Rapidly in Situ-Forming Degradable Hydrogels from Dextran Thiols through Michael Addition, Biomacromolecules 8 (5) (2007/05/01 2007,) 1548–1556, https://doi.org/10.1021/bm061191m.
[48] C.I. Torres, A. Kato Marcus, B.E. Rittmann, Proton transport inside the biofilm limits electrical current generation by anode-respiring bacteria, Biotechnol. Bioeng. 100 (5) (2008) 872–881, https://doi.org/10.1002/bit.21821.
[49] T.K.L. Meyvis, S.C. De Smedt, J. Demeester, W.E. Hennink, Influence of the Degradation Mechanism of Hydrogels on Their Elastic and Swelling Properties during Degradation, Macromolecules 33 (13) (2000/06/01 2000,) 4717–4725, https://doi.org/10.1021/ma992131u.
[50] S. Rojas-Flores, M. De La Cruz Noriega, S.M. Benites, G. Aguirre Gonzales, A. Salvador Salinas, F. Silva Palacios, Generation of bioelectricity from fruit waste, Energy Rep. 6 (2020/12/01/ 2020,) 37–42, https://doi.org/10.1016/j.egyr.2020.10.025.
[51] Y. Fan, H. Hu, H. Liu, Sustainable Power Generation in Microbial Fuel Cells Using Bicarbonate Buffer and Proton Transfer Mechanisms, Environmental Science & Technology 41 (23) (2007/12/01 2007,) 8154–8158, https://doi.org/10.1021/es071739c.
[52] E. Axpe, D. Chan, G.S. Offeddu, Y. Chang, D. Merida, H.L. Hernandez, E.A. Appel, A Multiscale Model for Solute Diffusion in Hydrogels, Macromolecules 52 (18) (2019) 6889–6897.
[53] P. Vanýsek, "Ionic Conductivity and Diffusion at Infinite Dilution," in *Handbook of Chemistry and Physics*, 1992/93 edition ed. Boca Raton: CRC Press, 1992, ch. 5, pp. 111-113.
[54] A. Cavallo, M. Madaghiele, U. Masullo, M. G. Lionetto, and A. Sannino, "Photo-crosslinked poly(ethylene glycol) diacrylate (PEGDA) hydrogels from low molecular weight prepolymer: Swelling and permeation studies," *Journal of Applied Polymer Science,* vol. 134, no. 2, 2017, doi: https://doi.org/10.1002/app.44380.
[55] P.S. Bonanni, D.F. Bradley, G.D. Schrott, J.P. Busalmen, Limitations for Current Production in Geobacter sulfurreducens Biofilms, ChemSusChem 6 (4) (2013) 711–720, https://doi.org/10.1002/cssc.201200671.
[56] V. Sapireddy, K.P. Katuri, A. Muhammad, P.E. Saikaly, Competition of two highly specialized and efficient acetoclastic electroactive bacteria for acetate in biofilm anode of microbial electrolysis cell, npj Biofilms Microbiomes 7 (1) (2021/05/31 2021,) 47, https://doi.org/10.1038/s41522-021-00218-3.
[57] R. Bansal, R.A. Helmus, B.A. Stanley, J. Zhu, L.J. Liermann, S.L. Brantley, M. Tien, Survival During Long-Term Starvation: Global Proteomics Analysis of Geobacter sulfurreducens under Prolonged Electron-Acceptor Limitation, J. Proteome Res. 12 (10) (2013) 4316–4326.

[58] B.R. Dhar, H. Ren, J. Chae, H.-S. Lee, Recoverability of electrical conductivity of a Geobacter-enriched biofilm, J. Power Sources 402 (2018/10/31/ 2018,) 198–202, https://doi.org/10.1016/j.jpowsour.2018.09.039.
[59] X. He, G. Chadwick, F. Jiménez Otero, V. Orphan, C. Meile, "Spatially Resolved Electron Transport through Anode-Respiring Geobacter sulfurreducens Biofilms, Controls and Constraints," *ChemElectroChem* 8 (10) (2021) 1747–1758, https://doi.org/10.1002/celc.202100111.
[60] J. An, H.-S. Lee, Implication of endogenous decay current and quantification of soluble microbial products (SMP) in microbial electrolysis cells, RSC Adv. 3 (33) (2013) 14021.
[61] C.E. Reimers, M. Wolf, Y. Alleau, C. Li, Benthic microbial fuel cell systems for marine applications, J. Power Sources 522 (2022/02/28/ 2022,), 231033, https://doi.org/10.1016/j.jpowsour.2022.231033.
[62] Y. Yan, T. Li, L. Zhou, L. Tian, X. Yan, C. Liao, Z. Huang, N. Li, X. Wang, Spatially heterogeneous propionate conversion towards electricity in bioelectrochemical systems, J. Power Sources 449 (2020) 227557.
[63] C. Picioreanu, M.C.M. van Loosdrecht, J.J. Heijnen, Modelling the effect of oxygen concentration on nitrite accumulation in a biofilm airlift suspension reactor, Water Sci. Technol. 36 (1) (1997/01/01/ 1997,) 147–156, https://doi.org/10.1016/S0273-1223(97)00347-8.
[64] E.H. Sanjaya, H. Cheng, Y.-Y. Li, Mesophilic methane fermentation performance and ammonia inhibition of fish processing wastewater treatment using a self-agitated anaerobic baffled reactor, Bioresour. Technol. 313 (2020/10/01/ 2020,), 123644, https://doi.org/10.1016/j.biortech.2020.123644.
[65] J.R. Kim, Y. Zuo, J.M. Regan, B.E. Logan, Analysis of ammonia loss mechanisms in microbial fuel cells treating animal wastewater, Biotechnol. Bioeng. 99 (5) (2008) 1120–1127, https://doi.org/10.1002/bit.21687.
[66] R.C. Tice, Y. Kim, Influence of substrate concentration and feed frequency on ammonia inhibition in microbial fuel cells, J. Power Sources 271 (2014/12/20/ 2014,) 360–365, https://doi.org/10.1016/j.jpowsour.2014.08.016.
[67] B. Virdis, S.T. Read, K. Rabaey, R.A. Rozendal, Z. Yuan, J. Keller, Biofilm stratification during simultaneous nitrification and denitrification (SND) at a biocathode, Bioresour. Technol. 102 (1) (2011/01/01/ 2011,) 334–341, https://doi.org/10.1016/j.biortech.2010.06.155.
[68] C.S. Dawes, H. Konig, C.C. Lin, Enzyme-immobilized hydrogels to create hypoxia for in vitro cancer cell culture, J Biotechnol 248 (2017) 25–34, https://doi.org/10.1016/j.jbiotec.2017.03.007.
[69] Y.E. Kim, J. Kim, ROS-Scavenging Therapeutic Hydrogels for Modulation of the Inflammatory Response, ACS Appl. Mater. Interfaces 14 (20) (2022) 23002–23021.
[70] B. Figdore, J. Tardio, T. Reid, M. J. Higgins, and M. Steele, "Solids Handling and Treatment Performance with Waste Activated Sludge from the NeredaÂ® Aerobic Granular Sludge Process: Comparisons to Conventional Activated Sludge," presented at the WEFTEC 2021, October, 2021.
[71] S. Cao, W. Yan, L. Yu, L. Zhang, W. Lay, Y. Zhou, Challenges of THP-AD centrate treatment using partial nitritation-anammox (PN/A) – inhibition, biomass washout, low alkalinity, recalcitrant and more, 117555, Water Res. 203 (2021), https://doi.org/10.1016/j.watres.2021.117555.
[72] B.E. Rittmann, The membrane biofilm reactor: the natural partnership of membranes and biofilm, Water Science and Technology 53 (3) (2006) 219–225.